Journal of Electroanalytical Chemistry 744 (2015) 32–36

Contents lists available at ScienceDirect

Journal of Electroanalytical Chemistry

journal homepage: www.elsevier.com/locate/jelechem

# Surface modification of $RuO_2$ nanoparticles–carbon nanofiber composites for electrochemical capacitors

Geon-Hyoung An, Hyo-Jin Ahn *

*Department of Materials Science and Engineering, Seoul National University of Science and Technology, Seoul 139-743, Republic of Korea*

ARTICLE INFO

*Article history:*
Received 10 December 2014
Received in revised form 26 February 2015
Accepted 4 March 2015
Available online 5 March 2015

*Keywords:*
Electrochemical capacitors
Surface modification
Nanostructured composites
Ruthenium oxide
Carbon nanofibers

ABSTRACT

Surface-modified $RuO_2$ nanoparticles–carbon nanofiber (CNF) composites are synthesized using electrospinning and acid treatment in sequence, and their structure, morphology, chemical states, and electrochemical performance are demonstrated. The surface-modified $RuO_2$–CNF composites exhibited the highest specific capacitance of 224.6 F $g^{-1}$, high-rate performance with capacitance retention of 80%, superior energy density of 26.9–21.5 Wh $kg^{-1}$, and excellent cycling stability of 90% after up to 3000 cycles, compared to the conventional CNFs, surface-modified CNFs, and unmodified $RuO_2$ nanoparticles–CNF composites. Their improved electrochemical performance can be explained as synergistic effect of well-distributed $RuO_2$ nanoparticles within the matrix of CNFs and surface modification induced by the increased number of oxygen-containing functional groups, which results in increased capacitance and improved high-rate performance due to Faradaic redox reactions and improved wettability.



## 1. Introduction

Electrochemical capacitors (ECs) have attracted great interest for various applications, such as in electronics, electric hybrid vehicles, and industrial power management, owing to their high power density, fast energy-storage ability, long cycle life, and broad range of working temperatures, compared to conventional secondary batteries [1–6]. Since the electrochemical performance of ECs directly depends on the properties of the electrode materials, the development of electrode materials having high capacitance, high-rate performance, and long cycle life can be considered as the key technology for high-performance ECs. In particular, in terms of different energy-storage mechanisms, ECs can be generally divided into two types: electric double-layer capacitors (EDLCs) and pseudo-capacitors. EDLCs are based on the accumulation of electrostatic charges in the electric double-layer between the electrode and the electrolyte. Carbon-based materials, such as activated carbon, graphene, carbon nanotubes (CNTs), and carbon nanofibers (CNFs) are usually used as electrodes in EDLCs due to their unique properties, such as low cost, large surface area, and physical/chemical stability [7–9]. Despite these advantages, the use of carbon materials for ECs is limited because of their low charge-storage capability. On the other hand, compared to EDLCs, pseudo-capacitors possess much higher charge-storage capability between the electrode and the electrolyte due to Faradaic redox reactions [10,11]. The typical electrode materials of pseudo-capacitors are transition-metal oxides (e.g., $RuO_2$, $Co_3O_4$, $MnO_2$, $V_2O_5$, and NiO) and conducting polymers (e.g., polyaniline, polythiophene, and polypyrrole) [12]. Although they have high charge-storage capability, disadvantages, such as high cost, particle aggregation of transition-metal oxides and conducting polymers, and relatively low electronic conductivity limit their application rang.

Many efforts have been made to conquer the above-mentioned disadvantages of carbon materials and transition-metal oxides. One of the strategies is to synthesize composite structures consisting of carbon materials and transition-metal oxides. For example, Ramakrishnan et al. [13] synthesized metallic cobalt nanoparticles embedded within carbon nanorods using electrospinning, which exhibited a specific capacitance of 146 $Fg^{-1}$ with good cycling stability. Another approach is to surface-modify the electrode materials using acid treatments [14,15]. For example, Li et al. [16] investigated activated CNTs using the mixed acid composed of $H_2SO_4$ and $HNO_3$, resulting in an electrode with a specific capacitance of 56.5 $Fg^{-1}$. However, a systematic study on $RuO_2$ nanoparticles–CNF composites combined with surface modification for high-performance ECs has not been performed until now. Thus, we synthesized a novel structure relative to the existing surface-modified $RuO_2$ nanoparticles–CNF composites by applying electrospinning and acid treatment in sequence. The CNFs were chosen as matrix of the composite electrodes due to their low cost, high surface area-to-volume ratio (462 $m^2$ $g^{-1}$), superb electrical

* Corresponding author.
*E-mail address:* hjahn@seoultech.ac.kr (H.-J. Ahn).

http://dx.doi.org/10.1016/j.jelechem.2015.03.009
1572-6657/

conductivity ($10^2$ S cm$^{-1}$), and excellent chemical/physical stability, as well as the network of nanostructures causing efficient electron transport [17–20].

## 2. Experimental details

### 2.1. Chemicals

Polyacrylonitrile (PAN, $M_w$ = 150,000), ruthenium (III) chloride hydrate ($RuCl_3{\cdot}xH_2O$), polyvinylpyrrolidone (PVP, $M_w$ = 1,300,000), N,N-dimethylformamide (DMF, 99.8%), nitric acid (70%), and N-methyl-2-pyrrolidinone (NMP, 99.5%) were purchased from Sigma–Aldrich. All chemicals were used without further purification.

### 2.2. Synthesis of surface-modified $RuO_2$–CNF composites

Surface-modified $RuO_2$ nanoparticles–CNF composites were synthesized using electrospinning and acid treatment in sequence. For comparison, we prepared four different types of electrode materials, namely conventional CNFs, surface-modified CNFs, $RuO_2$ nanoparticles–CNF composites, and surface-modified $RuO_2$ nanoparticles–CNF composites. First, 7 wt% PAN, 3 wt% $RuCl_3{\cdot}xH_2O$, and 4 wt% PVP were dissolved in DMF under vigorous stirring for 5 h. For proper electrospinning conditions, the working voltage and feeding rate were maintained at 13 kV and 0.03 mL/h, respectively. The distance between the syringe needle and collector was set at 15 cm under 10% humidity in the chamber. The as-spun nanofibers were stabilized at 280 °C for 2 h in air and then carbonized at 800 °C for 2 h under $N_2$ gas (99.999%) to obtain the $RuO_2$–CNF composites. The resultant composites were oxidized for the formation of oxygen-containing functional groups, such as C–O, C=O, and O–C=O groups at the surfaces using an $HNO_3$ solution for 5 h. The surface-modified composites were washed several times with de-ionized (DI) water and then dried in an oven at 80 °C, finally resulting in the preparation of surface-modified $RuO_2$–CNF composites. In addition, conventional CNFs were prepared without Ru precursor and the surface-modified CNFs were prepared using the above-mentioned acid treatment.

### 2.3. Characterization

Field-emission scanning electron microscopy (FESEM, Hitachi S-4800) and transmission electron microscopy (TEM; Tecnai $G^2$, KBSI Gwangju Center) were used to investigate the structure and morphology of the samples. TEM–EDS mapping was performed by a Phillips CM20T/STEM equipped with an energy-dispersive X-ray spectrometer (EDS). The contents of the samples were characterized by thermogravimetric analysis (TGA-50, Shimadzu) in the temperature range from 100 to 500 °C at a heating rate of 10 °C min$^{-1}$ in air atmosphere. The crystallinity and the chemical bonding states of the samples were examined by X-ray diffraction (XRD, Rigaku D/MAX2500V) with Cu Kα radiation in the angular range from 10° to 90° with a step size of 0.02° and X-ray photoelectron spectroscopy (XPS, ESCALAB250) employing an Al Kα X-ray source under a base pressure of 267 nPa.

### 2.4. Electrode preparation and electrochemical measurements

Electrochemical measurements were performed using a symmetric two-electrode system with 6 M KOH solution as electrolyte. The prepared samples were mixed with Ketjen black (Mitsubishi Chemical, ECP-600JD) as conducting material and poly(vinylidene difluoride) (PVDF, Alfa Aesar) as binder in the weight ratio of 8:1:1. The slurry, which was prepared in NMP as solvent, was coated on Ni foam with size of 1 cm × 1 cm and the resultant electrodes were dried in air at 100 °C for 12 h. The mass and thickness of the electrodes were fixed at 10 mg and 0.1 mm, respectively. Cyclic voltammetry (CV) measurements were performed using a potentiostat/galvanostat (Autolab PGSTAT302N, FRA32M) in the potential range of 0.0–1.0 V at the scan rate of 10 mV s$^{-1}$. The galvanostatic charge/discharge measurements were demonstrated at a current density of 0.2–10 A g$^{-1}$ in a voltage range of 0.0–1.0 V using a battery cycler system (WonA Tech., WMPG 3000). The cycling stability of the cells was investigated for up to 3000 cycles at the current density of 1 A g$^{-1}$.

## 3. Results and discussion

Fig. 1 shows FESEM images of the conventional CNFs, surface-modified CNFs, $RuO_2$–CNF composites, and surface-modified $RuO_2$–CNF composites. All samples exhibit smooth surfaces and uniform morphologies. The average diameters of the samples are estimated to be about 274–296 nm for the conventional CNFs (Fig. 1a), 265–289 nm for surface-modified CNFs (Fig. 1b), 213–221 nm for $RuO_2$–CNF composites (Fig. 1c), and 212–219 nm for surface-modified $RuO_2$–CNF composites (Fig. 1d). In particular, the diameters of the untreated and surface-modified $RuO_2$–CNF composites are smaller than those of the conventional and surface-modified CNFs. The reason for the different average size is the slight consumption of CNFs during the carbonization process because of the partial oxidation–reduction reaction between the Ru precursor and PVP polymer [21,22]. Furthermore, both the untreated and surface-modified $RuO_2$–CNF composites display the formation of uniform nanofibers without any beads of agglomerated $RuO_2$ on the CNF surface, which implies that the $RuO_2$ nanoparticles were totally embedded within the CNF matrix.

The structure and morphology of the individual samples were further analyzed by TEM. Fig. 2 shows low-resolution ((a)–(d)) and high-resolution ((e)–(h)) TEM images of the conventional CNFs, surface-modified CNFs, $RuO_2$–CNF composites, and surface-modified $RuO_2$–CNF composites. The conventional CNFs (Fig. 2a and e) and surface-modified CNFs (Fig. 2b and f) exhibit

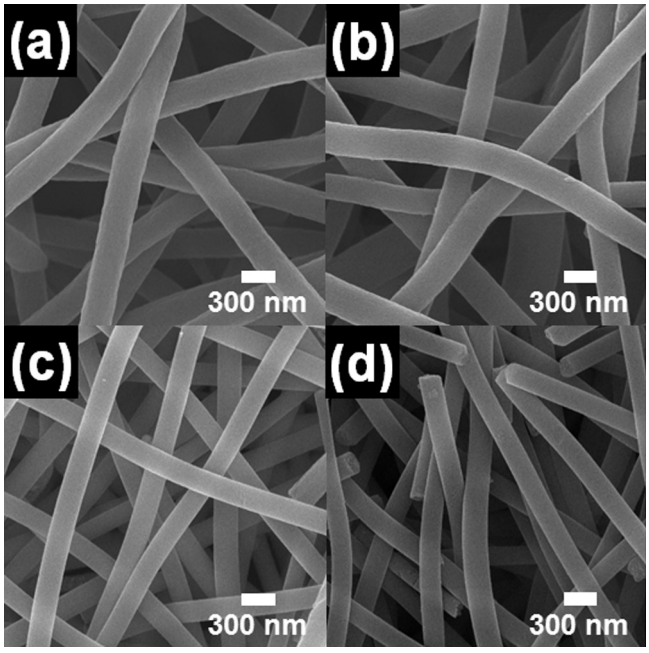


**Fig. 1.** FESEM images of the conventional CNFs, surface-modified CNFs, untreated $RuO_2$–CNF composites, and surface-modified $RuO_2$–CNF composites.

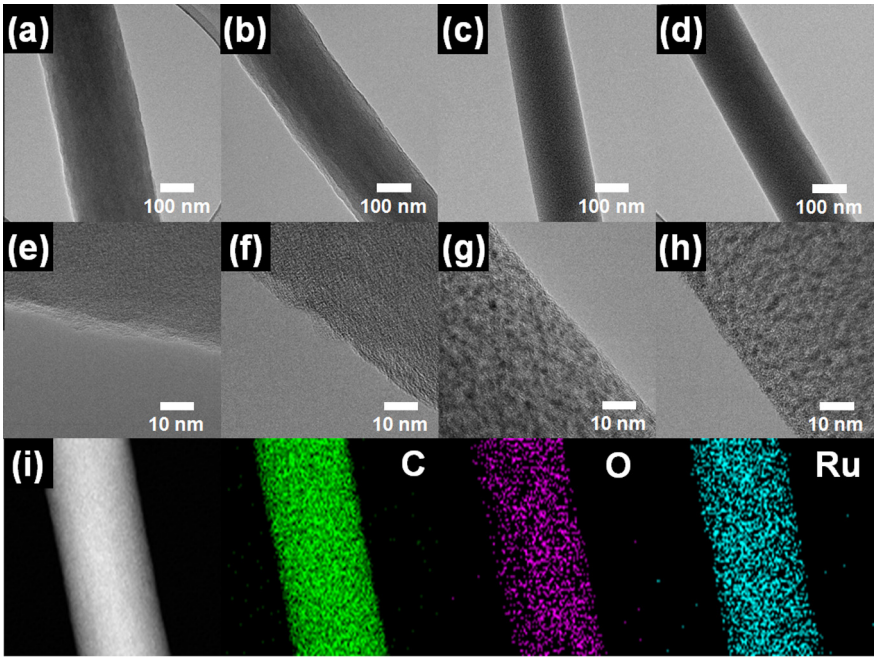


**Fig. 2.** Low-resolution ((a)–(d)) and high-resolution ((e)–(h)) TEM images of the conventional CNFs, surface-modified CNFs, untreated $RuO_2$–CNF composites, and surface-modified $RuO_2$–CNF composites. (i) TEM–EDS mapping data obtained from surface-modified $RuO_2$–CNF composites.

a uniform contrast because there exists only a single phase in these CNFs, whereas the untreated (Fig. 2c and g) and surface-modified $RuO_2$–CNFs (Fig. 2d and h) composites display non-uniform contrast owing to the existence of $RuO_2$ nanoparticles in the CNF matrix. In addition, the two samples show well-distributed $RuO_2$ nanoparticles with 2–3 nm in size inside of the CNF matrix. Therefore, these results imply that the structure and morphology of the surface-modified composites is not strongly modified by the acid-treatment. Fig. 2i presents TEM–EDS mapping data obtained from surface-modified $RuO_2$–CNF composites to confirm the well-distribution of Ru atoms in the CNF matrix. The EDS results indicate that Ru atoms are uniformly dispersed in the CNF matrix.

To further investigate the contents and thermal stability of the untreated and surface-modified $RuO_2$–CNF composites, TGA analysis from 100 to 500 °C at a heating rate of 10 °C $min^{-1}$ was carried out in air atmosphere, as shown in Fig. 3. The untreated and surface-modified $RuO_2$–CNF composites exhibited a weight loss of 26.2% and 25.8%, respectively. The similar weight loss of the two samples is attributed to almost the same amount of $RuO_2$ nanoparticles.

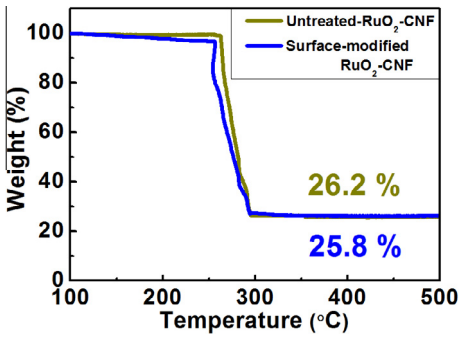


**Fig. 3.** TGA curves of the conventional CNFs, surface-modified CNFs, untreated $RuO_2$–CNF composites, and surface-modified $RuO_2$–CNF composites from 100 to 500 °C at a heating rate of 10 °C $min^{-1}$ in air atmosphere.

Fig. 4a shows XRD patterns of all samples to examine their crystallographic structure and degree of crystallinity. The reference reflection of the pure $RuO_2$ phase (JCPDS card No. 88-0322) is shown at the bottom of Fig. 4a. The conventional and surface-modified CNFs exhibit only a broad peak around 25°, corresponding to the (0 0 2) reflection of graphite. Concerning the untreated and surface-modified $RuO_2$–CNF composites, the corresponding XRD patterns exhibit the main diffraction peak at 28.0°, corresponding to the (1 1 0) plane of the $RuO_2$ phase with tetragonal structure (space group $P4_2/mnm$ [136]). To verify the chemical bonding states of the CNF and $RuO_2$ phase of the surface-modified composites, XPS measurements were performed, as shown in Fig. 4b and d. The decomposition of the C1s spectra of untreated and surface-modified $RuO_2$–CNF composites (Fig. 4b and c) results in intensities at 284.5 eV, 286.0 eV, 287.4 eV, and 288.9 eV, which correspond to C–C groups, C–O groups, C=O groups, and O–C=O groups, respectively [23]. The C–O and C=O groups correspond to hydroxyl (–OH) and the O–C=O groups correspond to carboxyl (–COOH) groups. Table 1 summarizes the percentages of several oxygen-containing functional groups at the surface of the untreated and surface-modified $RuO_2$–CNF composites. The results evidence an enhancement in the number of oxygen-functional groups relative to the number of carboxyl groups at the composite surface after the acid treatment. The percentage of carboxyl groups of the untreated and surface-modified $RuO_2$–CNF composites was 6.5% and 10.9%, respectively. The increased number of oxygen-containing functional groups can provide better electrochemical performance in ECs compared to carbon–carbon groups due to synergistic effects of pseudo-capacitance and improved wettability resulting in improved ion transport properties, in particular at high current density [24,25]. Fig. 4d displays Ru 3*p* core-level spectra from Ru $3p_{3/2}$ and Ru $3p_{1/2}$ photoelectrons, observed at 464.0 eV and 486.7 eV, respectively. This implies that the Ru ions of the $RuO_2$ phase exist in form of Ru(IV) states [26]. Thus, the FESEM, TEM, XRD, and XPS results indicate the successful synthesis of surface-modified $RuO_2$ nanoparticles–CNF composites. Fig. 4e presents a schematic illustration of ideal composites of surface-modified $RuO_2$ nanoparticles and CNFs.

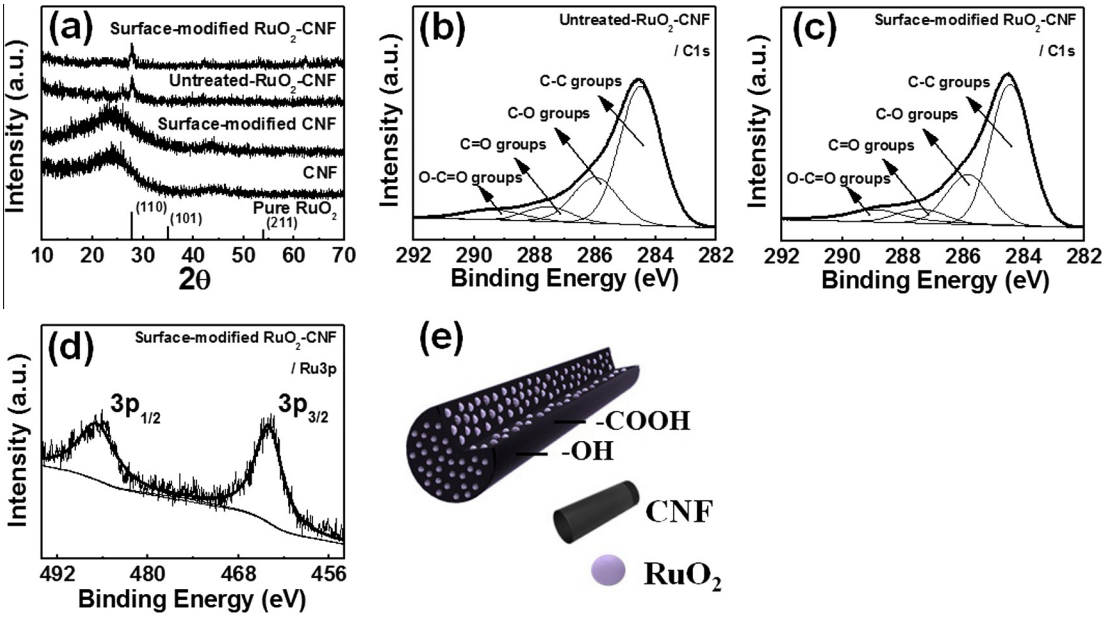


**Fig. 4.** (a) XRD patterns of the conventional CNFs, surface-modified CNFs, untreated $RuO_2$–CNF composites, and surface-modified $RuO_2$–CNF composites. (b) XPS spectra of C1s of untreated $RuO_2$–CNF composites. (c) XPS spectra of C1s of surface-modified $RuO_2$–CNF composites. (d) XPS core-level spectra of Ru $3p_{3/2}$ and Ru $3p_{1/2}$ of surface-modified $RuO_2$–CNF composites. (e) A schematic illustration of ideal composites of surface-modified $RuO_2$ nanoparticles and CNFs.

**Table 1**
Percentages of several oxygen-containing functional groups on the surfaces of untreated $RuO_2$–CNF composites, and surface-modified $RuO_2$–CNF composites before and after the acid treatment.

| Samples | C–C (284.5 eV) Concentration (%) | C–O (286.0 eV) Concentration (%) | C=O (287.4 eV) Concentration (%) | O–C=O (288.9 eV) Concentration (%) |
|---|---|---|---|---|
| Untreated $RuO_2$/CNF | 64 | 22.3 | 7.2 | 6.5 |
| Surface modified $RuO_2$/CNF | 59 | 22.9 | 7.2 | 10.9 |

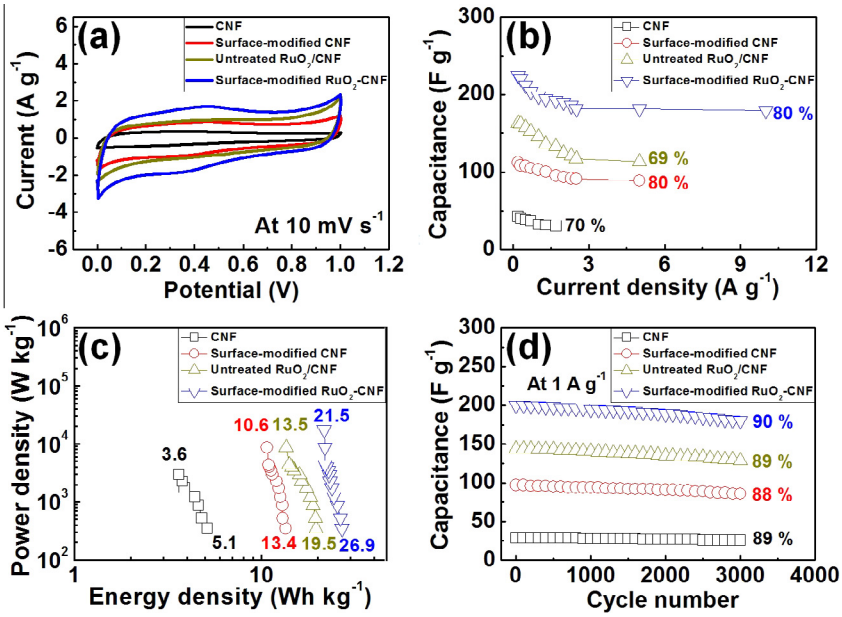


**Fig. 5.** (a) Cyclic voltammetry (CV) measurements of all electrodes at the scan rate of 10 mV $s^{-1}$ in a voltage range of 0.0–1.0 V. (b) Specific capacitance at a current density of 0.2–10 A $g^{-1}$. (c) A Ragone plot of all electrodes in the power density range from 349.0–17454.5 W $kg^{-1}$. (d) Cycling stability at a current density of 1 A $g^{-1}$ for up to 3000 cycles.

To examine the electrochemical properties of all electrodes, CV measurements were performed by a potentiostat/galvanostat in the potential range of 0.0–1.0 V at the scan rate of 10 mV $s^{-1}$ in aqueous 6M KOH, as shown in Fig. 5a. In particular, the surface-modified $RuO_2$–CNF composite electrode showed a larger quasi-rectangular curve, which means that it possesses excellent

capacitive properties. Moreover, the broad peaks at 0.4–0.5 V in CV indicate a pseudo-capacitance behavior corresponding to Faradaic redox reactions owing to the co-existence of $RuO_2$ nanoparticles embedded within the CNFs and enhanced oxygen-containing functional groups at the surfaces. The specific capacitance of the electrodes was calculated by the following equation [27,28]:

$$C_{sp} = 4I/(mdV/dt) \quad (1)$$

where $I$ is the current (A), $m$ is the total mass of the active material (g), $V$ is the voltage window (V), and $t$ is the discharging time (s). As shown in Fig. 5b, the specific capacitances of conventional CNF, surface-modified CNF, $RuO_2$–CNF composite, and surface-modified $RuO_2$–CNF composite electrodes at the current density of 0.2 A $g^{-1}$ are 44.8, 112.4, 163.2, and 224.6 F $g^{-1}$, respectively. The surface-modified $RuO_2$–CNF electrode indicated superior specific capacitance at all current densities among the electrodes investigated in this study, ascribed to synergistic effects arising from the co-existence of well-distributed $RuO_2$ nanoparticles in CNFs and an enhanced number of oxygen-containing functional groups at the surfaces. In addition, the specific capacitances of all electrodes decrease sharply with increasing current density due to the reduced ion diffusion time during the charge/discharge process. Nevertheless, the surface-modified $RuO_2$–CNF composite electrode exhibited excellent high-rate performance with the specific capacitance of 179.2 F $g^{-1}$ even at the high current density of 10 A $g^{-1}$ and the retention of 80%, owing to the improved wettability. At high current density, the oxygen-containing functional groups are easily accessible to the ions [25].

In the Ragone plot (Fig. 5c), the energy density ($E$, Wh $kg^{-1}$) and power density ($P$, W $kg^{-1}$) were evaluated on the basis of the galvanostatic charge/discharge measurements using a two-electrode system by the following equation [29]:

$$E = C_{sp}V^2/8 \quad (2)$$

$$P = E/dt \quad (3)$$

where $C_{sp}$, $V$, and $dt$ are the specific capacitance of the two-electrode system, the discharge voltage, and total discharge time, respectively. Accordingly, the Ragone plots show a reduction of the energy density with increasing power density. The energy density of the surface-modified $RuO_2$–CNF composite electrode exhibits 26.9–21.5 Wh $kg^{-1}$ in the power density range from 349.0–17454.5 W $kg^{-1}$, implying superior energy density among the presently investigated electrodes. In addition, as shown in Fig. 5d, the surface-modified $RuO_2$–CNF composite electrode displays excellent cycling stability, namely, it exhibits the capacitance retention of 90% during 3000 cycles at 1 A $g^{-1}$.

The superb electrochemical performance of the surface-modified $RuO_2$–CNF composite electrode can be explained by two major reasons. One is the existence of well-dispersed $RuO_2$ nanoparticles in CNFs leading to increased capacitance by Faradaic redox reactions. The other is the formation of an enhanced number of oxygen-containing functional groups (–COOH groups) at the surfaces which results in the excellent high-rate performance based on the enhanced wettability as well as the increased capacitance using the Faradiac redox reactions. Therefore, surface-modified $RuO_2$–CNF composites with improved electrochemical properties represent a promising electrode material for use in high-performance ECs.

## 4. Conclusion

Surface-modified $RuO_2$–CNF composites for use as electrodes in ECs were synthesized using electrospinning and acid treatment in sequence. $RuO_2$ nanoparticles having 2–3 nm in size were uniformly embedded within the surface-modified CNFs. After the acid treatment, the amount of oxygen-containing functional groups (–COOH groups) at the CNF surface increased by up to 10.9%. The surface-modified $RuO_2$–CNF composites exhibited superior specific capacitance of 224.6 F $g^{-1}$ at the current density of 0.2 A $g^{-1}$, high-rate performance with a capacitance retention of 80%, superb energy density of 26.9–21.5 Wh $kg^{-1}$, and excellent cycling stability for up to 3000 cycles. The superior electrochemical properties become evident by the comparison to conventional CNFs, surface-modified CNFs, and untreated $RuO_2$–CNF composites. Thus, the excellent electrochemical performance is based on the synergistic effect of well-distributed $RuO_2$ nanoparticles within the CNFs and the increased number of oxygen-containing functional groups at the CNF surfaces.

## Acknowledgments

This research was supported by Basic Science Research Program through the National Research Foundation of Korea (NRF) funded by the Ministry of Education, Science and Technology (2012-007444).

## References

[1] P. Simon, Y. Gogotsi, B. Dunn, Science 343 (2014) 1210–1211.
[2] P. Simon, Y. Gogotsi, Nat. Mater. 7 (2008) 845–854.
[3] G.-H. An, H.-J. Ahn, W.-K. Hong, J. Power Sources 274 (2015) 536–541.
[4] J. Huang, S. Yang, Y. Xu, X. Zhou, X. Jiang, N. Shi, D. Cao, J. Yin, G. Wang, J. Electroanal. Chem. 713 (2014) 98–102.
[5] J. Cao, Y. Wang, Y. Zhou, D. Jia, J.-H. Ouyang, L. Guo, J. Electroanal. Chem. 682 (2012) 23–28.
[6] J. Sanchez-Gonzalez, F. Stoeckli, T.A. Centeno, J. Electroanal. Chem. 657 (2011) 176–180.
[7] G.-H. An, H.-J. Ahn, Electrochem. Solid-State Lett. 3 (2014) M29–M32.
[8] G.-H. An, H.-J. Ahn, J. Power Sources 272 (2014) 828–836.
[9] G.-H. An, H.-J. Ahn, Ceram. Int. 38 (2012) 3197–3201.
[10] S. Vijayakumar, G. Muralidharan, J. Electroanal. Chem. 727 (2014) 53–58.
[11] G.-H. An, H.-J. Ahn, Electrochem. Solid-State Lett. 2 (2013) M33–M36.
[12] G. Yu, X. Xie, L. Pan, Z. Bao, Y. Cui, Nano Energy 2 (2013) 213–234.
[13] P. Ramakrishnan, S. Shanmugam, Electrochim. Acta 125 (2014) 232–240.
[14] H.-R. Yu, S. Cho, M.-J. Jung, Y.-S. Lee, Micropor. Mesopor. Mater. 172 (2013) 131–135.
[15] M.-J. Jung, E. Jeong, S. Cho, S.Y. Yeo, Y.-S. Lee, J. Colloid Interface Sci. 381 (2012) 152–157.
[16] C. Li, D. Wang, T. Liang, X. Wang, L. Ji, Mater. Lett. 58 (2004) 3774–3777.
[17] G.-H. An, H.-J. Ahn, Carbon 65 (2013) 87–96.
[18] B. Zhao, S. Jiang, C. Su, R. Cai, R. Ran, M.O. Tadé, Z. Shao, J. Mater. Chem. A 1 (2013) 12310–12320.
[19] G.-H. An, H.-J. Ahn, J. Electroanal. Chem. 707 (2013) 74–77.
[20] M. Zhang, E. Uchaker, S. Hu, Q. Zhang, T. Wang, G. Cao, J. Li, Nanoscale 5 (2013) 12342–12349.
[21] Z. Yang, G. Du, Z. Guo, X. Yu, S. Li, Z. Chen, P. Zhanga, H. Liua, Nanoscale 2 (2010) 1011–1017.
[22] G.-H. An, S.-J. Kim, K.-W. Park, H.-J. Ahn, Electrochem. Solid-State Lett. 3 (2014) M21–M23.
[23] A.P. Terzyk, Colloids Surf. A Physicochem. Eng. Aspects 177 (2001) 23–45.
[24] X. Fan, Y. Lu, H. Xu, X. Kong, J. Wang, J. Mater. Chem. 21 (2011) 18753–18760.
[25] C. Ma, Y. Li, J. Shi, Y. Song, L. Liu, Chem. Eng. J. 249 (2014) 216–225.
[26] K.C. Park, I.Y. Jang, W. Wongwiriyapan, S. Morimoto, Y.J. Kim, Y.C. Jung, T. Toyad, M. Endo, J. Mater. Chem. 20 (2010) 5345–5354.
[27] M. Liu, W.W. Tjiu, J. Pan, C. Zhang, W. Gao, T. Liu, Nanoscale 6 (2014) 4233–4242.
[28] X. Li, W. Xing, S. Zhuo, J. Zhou, F. Li, S.-Z. Qiao, G.-Q. Lu, Bioresour. Technol. 102 (2011) 1118–1123.
[29] X. Yang, L. Zhang, F. Zhang, T. Zhang, Y. Huang, Y. Chen, Carbon 72 (2014) 381–386.